

Article

# Effect of Deformation on Safety and Capacity of Li-Ion Batteries

Genwei Wang <sup>1,2,\*</sup>, Juanjuan Wu <sup>2,3</sup>, Zijun Zheng <sup>2,3</sup>, Lingeng Niu <sup>2,3</sup>, Lei Pan <sup>2,3</sup> and Bin Wang <sup>4,\*</sup> <sup>1</sup> College of Aeronautics and Astronautics, Taiyuan University of Technology, Jinzhong 030600, China<sup>2</sup> Shanxi Key Laboratory of Material Strength and Structure Impact, Taiyuan 030024, China<sup>3</sup> College of Mechanical and Vehicle Engineering, Taiyuan University of Technology, Taiyuan 030024, China<sup>4</sup> Department of Mechanical and Aerospace Engineering, Brunel University London, London UB8 3PH, UK

\* Correspondence: gwang@tyut.edu.cn (G.W.); bin.wang@brunel.ac.uk (B.W.)

**Abstract:** Deformations in lithium-ion batteries, which may lead to thermal runaway, can occur during storage and transportation handling, as well as in road use. In this study, both radial and axial compression deformation were produced experimentally to analyze their influence on the performance and safety of lithium-ion batteries. In the radial plate compression experiment, the battery was loaded to different displacements and then charge–discharge cycles were performed. It was found that the greater the deformation of the battery, the smaller the initial capacity and the faster the capacity decay. Under axial loading, the voltage of low state of charge (SOCs) batteries showed a clear step-drop phenomenon. The battery was compressed until the first voltage drop, loading was stopped, and the voltage gradually dropped to 0 V. For high-SOC lithium-ion batteries, there was almost no voltage step-down, and a small deformation could cause thermal runaway in the battery. The results showed that the small deformation in the radial direction only reduced the capacity of the battery, but had little impact on its safety, whereas a small deformation in the axial direction was more likely to cause an internal short circuit (ISC).



**Citation:** Wang, G.; Wu, J.; Zheng, Z.; Niu, L.; Pan, L.; Wang, B. Effect of Deformation on Safety and Capacity of Li-Ion Batteries. *Batteries* **2022**, *8*, 235. <https://doi.org/10.3390/batteries8110235>

Academic Editor: Binghe Liu

Received: 23 September 2022

Accepted: 8 November 2022

Published: 11 November 2022

**Publisher's Note:** MDPI stays neutral with regard to jurisdictional claims in published maps and institutional affiliations.



**Copyright:** © 2022 by the authors. Licensee MDPI, Basel, Switzerland. This article is an open access article distributed under the terms and conditions of the Creative Commons Attribution (CC BY) license (<https://creativecommons.org/licenses/by/4.0/>).

**Keywords:** deformation; lithium-ion battery safety; capacity attenuation; internal short circuit

## 1. Introduction

Lithium-ion batteries are often used in energy storage devices for electric vehicles (EVs) due to their long cycle life, high energy density, and high specific power. However, in recent years, electric vehicle accidents caused by battery damage have occurred frequently, causing serious losses to people's lives and properties. In order to ensure the safety of power batteries, relevant international organizations have formulated rules and regulations [1,2], and a large number of scholars have joined the research community on lithium-ion batteries.

Lithium-ion battery failure is mainly caused by electrical abuse, thermal abuse, and mechanical abuse; of these, mechanical abuse (for example, deformation, acupuncture, and collapse) is the most common cause of battery failure, and will affect battery safety. In view of this phenomenon, researchers have conducted a large number of experiments on lithium-ion batteries to study the deformation modes and failure mechanisms [3–9], such as quasi-static radial plate compression test, indentation test, axial compression test, dynamic impact test, drop weight test and so on. In addition, according to the structural and mechanical characteristics of the battery, the finite element model is established to predict the failure [10–14], which can provide a guarantee for the safe use of the battery. The experimental results show that both loading speed and battery SOC affect the safety of lithium-ion batteries [15–17], and power batteries with higher loading speed and SOC are more prone to thermal runaway. Thermal runaway is the most serious damage mode of power batteries, often caused by mechanical abuse; thermal runaway is irreversible and can easily occur. For lithium-ion batteries without thermal runaway, the failure of the battery is often judged by the voltage drop or load inflection point caused by an internal short circuit.

However, in some special cases, the battery does not show an obvious fault phenomenon, and the battery management system (BMS) cannot detect the degree of damage, which carries hidden security risks. For example, deformation that does not cause thermal runaway during storage, transportation, or use may cause potential damage to the battery and pose a hazard. In order to reduce the occurrence of accidents, it is important to determine the health of a battery. Li et al. [18] found that by establishing the relationship between battery capacity, temperature rise, deformation, and other parameters, the sensor network measurement values can be used to monitor the performance and safety of lithium-ion batteries. Spielbauer et al. [19] proposed a method to detect the damage and critical safety state of lithium-ion batteries under deforming mechanical abuse using electrochemical impedance spectroscopy. They found that local deformation does not cause an increase in electrochemical impedance spectrum, whereas large-area compression deformation causes an increase in ohmic resistance. Müller et al. [20] found that appropriate uniform pressure distribution is beneficial to battery performance and cycle life. Zhu et al. [21,22] studied the capacity loss mechanism of lithium-ion pocket cells induced by mechanical indentation using both *in situ* and non-*in situ* methods, and found that the indentation experiment would attenuate the battery capacity. In addition to the improvement of electrode materials [23,24], the electronic conductivity is also an important aspect for the capacity study. Yue et al. [25,26] provided basic insights into the electron conductivity, cycle durability, and rate capability of metal phosphide electrodes, and found that phosphorus doping has an indispensable role in significantly improving the electron conductivity and  $\text{Li}^+$  diffusion kinetics of  $\text{NiMoO}_4$  materials. Li et al. [27] studied the processes of lithiation and delithiation of lithium-ion batteries, and proposed strategies to optimize ion migration. Mallarapu et al. [28] found that during the deformation process, the ionic conductivity in the electrolyte decreased and the joule heating caused by ionic current increased significantly. However, there are few detailed studies on the influence of deformation on the safety and capacity of power batteries under quasi-static plate compression.

In this study, the quasi-static radial and axial loading of lithium-ion battery was performed, and the load, voltage, displacement, and other data during the loading process were recorded. Combined with the CT scanning technology, the deformation modes of the lithium-ion battery were analyzed along the two loading directions, and the influence of different deformations on battery capacity and safety performance was studied.

## 2. Preparations for Experiments

### 2.1. The Battery Information

A commercial ternary cylindrical lithium-ion battery with a height of 65 mm and a diameter of 18 mm was used in this study. The battery is composed of a shell, jellyroll, and steel core, and the positive cap has a pressure reducing valve, as shown in Figure 1. The jellyroll of the cylindrical battery is wound in the order of separator-negative-separator-positive, and the hard shell surrounding the jellyroll is made by stainless steel. The anode and cathode electrode materials are NCM523 and graphite, respectively, and the main electrolyte material is  $\text{LiPF}_6$ .

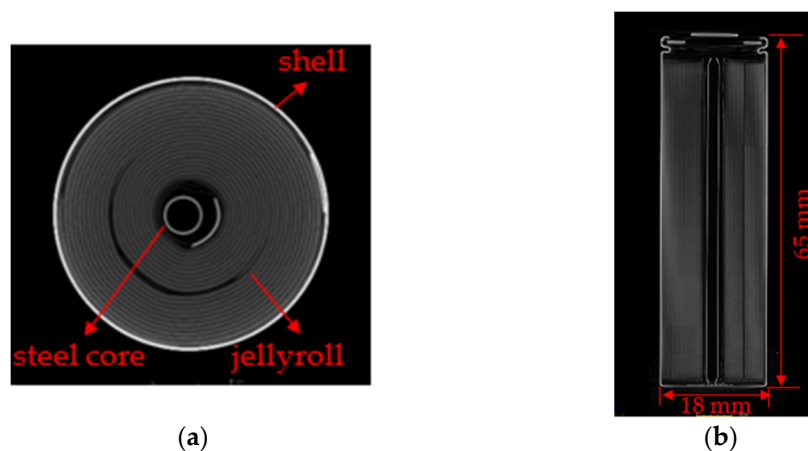


**Figure 1.** CT scan of 18650 lithium-ion battery: (a) cross section; (b) longitudinal section.

## 2.2. Introduction to the Experiment

Before the test, the LAND battery test instrument was used to charge the lithium-ion battery to the specified SOC according to the constant current–constant voltage (CC–CV) charging mode. The research showed that the CC–CV charging mode could achieve efficient charging while protecting batteries, and can provide detailed battery information [29]. The typical charging mode had the following order. First, the battery is charged to 4.2 V at a charging rate of 0.2 C, and then charged to a current of 0.02 C at a constant voltage of 4.2 V. Second, the battery is discharged to a voltage of 2.75 V at a discharge rate of 0.2 C and rested for 1 min. Finally, the battery is charged to a specified capacity at a charging rate of 0.2 C. Figure 2 shows the charging and discharging curves of the 80% SOC lithium-ion battery.

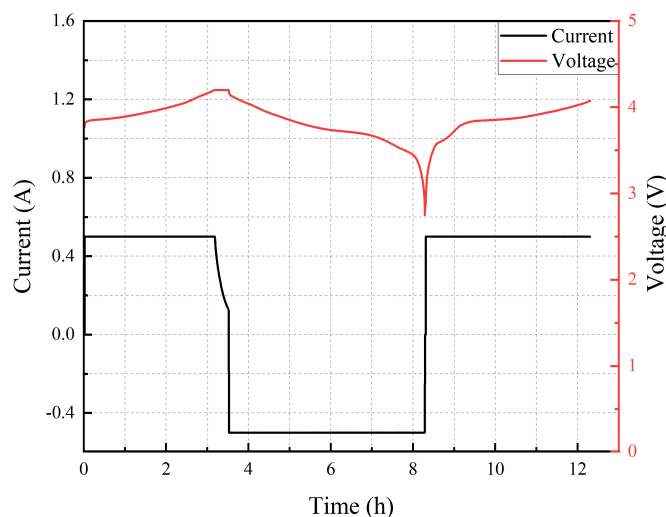


**Figure 2.** Charge and discharge curve of lithium–ion battery.

In the quasi-static radial compression test, a universal material testing machine (model: ETM 105D, wance Technologies Ltd., Shenzhen, China) was used for displacement loading, as shown in Figure 3. A digital oscilloscope (model: Tektronix TDS 2024C, Tektronix Inc., Beaverton, OR, USA) was used to record the voltage of the battery. An infrared thermal imager (model: Yoseen X640A600MF25, Wuhan Yoseen Infrared Co., Ltd., Wuhan, China) was used for the temperature changes.

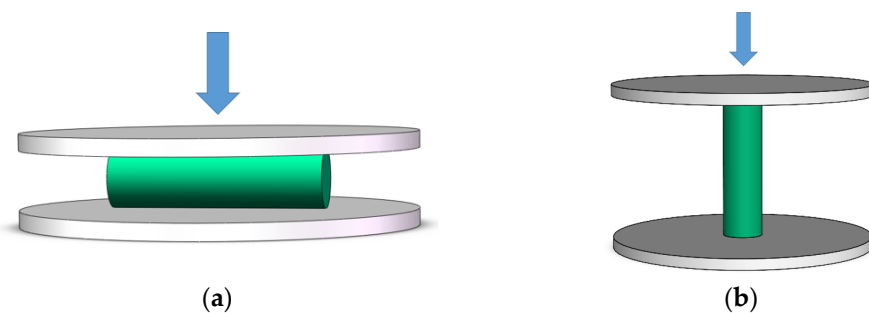


**Figure 3.** Loading conditions for lithium-ion batteries: (a) radial loading; (b) axial loading.

### 3. Results and Discussion

#### 3.1. Study on Radial Deformation Process

Quasi-static radial compression was performed on Li-ion batteries with different SOCs at a loading speed of 2 mm/min. Figure 4a shows the relationship between load, temperature, and voltage changes with loading displacement in the radial loading process of the 20% SOC Li-ion battery. Thus, the nominal stress  $\sigma$ , nominal strain  $\varepsilon$ , and nominal modulus  $E$  of the battery can be obtained. Nominal stress can be expressed as:

$$\sigma = \frac{F}{S} \quad (1)$$

where  $F$  is the load and  $S$  is the contact area between the battery and the platform during loading.  $S$  can be considered as:

$$S = b \cdot l \quad (2)$$

where  $b$  is the width of the contact area [14] and  $l$  is the axial length of the cylindrical battery. Then,  $b$  can be estimated via:

$$b = 2R \cdot \arccos\left(\frac{R - \delta}{R}\right) \quad (3)$$

where  $R$  is the radius of the battery and  $\delta$  is the loading displacement. Nominal strain  $\varepsilon$  can be obtained as:

$$\varepsilon = \frac{\delta}{2R} \quad (4)$$

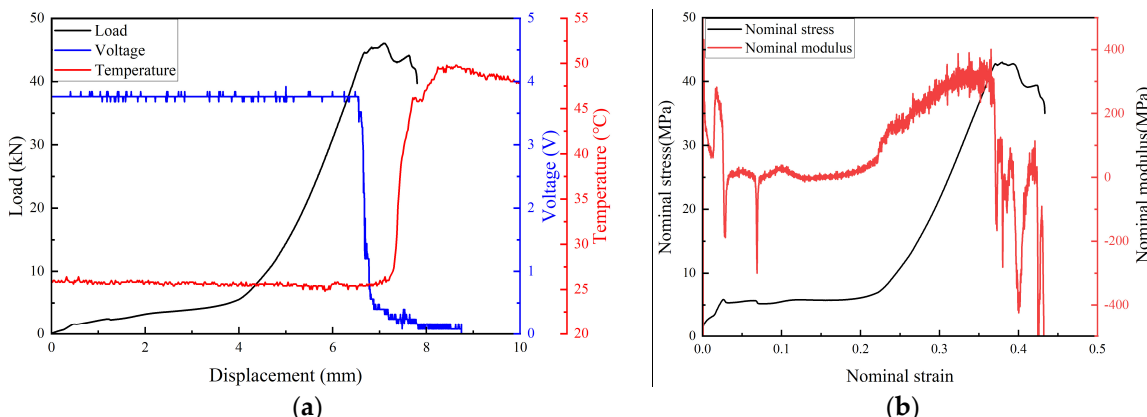


**Figure 4.** Loading curve of Li-ion battery: (a) load, voltage, temperature–displacement curve; (b) nominal stress, nominal modulus–nominal strain curves.

The nominal modulus E is obtained by:

$$E = \frac{d\sigma}{d\varepsilon} \quad (5)$$

It can be seen from Figure 4b that the stress–strain curve of the battery has three stages: the elastic stage followed by a plastic plateau stage, and the compaction stage, which yielded similar characteristics to porous materials.

In order to understand the characteristics of battery deformation, the positive cap of the lithium-ion battery was cut off and radial loading was performed, as shown in Figure 5. Figure 5a shows the load and nominal modulus–displacement curve of the battery; it is found that the peak load of the battery was similar to that of the complete battery, indicating that the positive cap had little effect on the load carrying capacity of the battery.

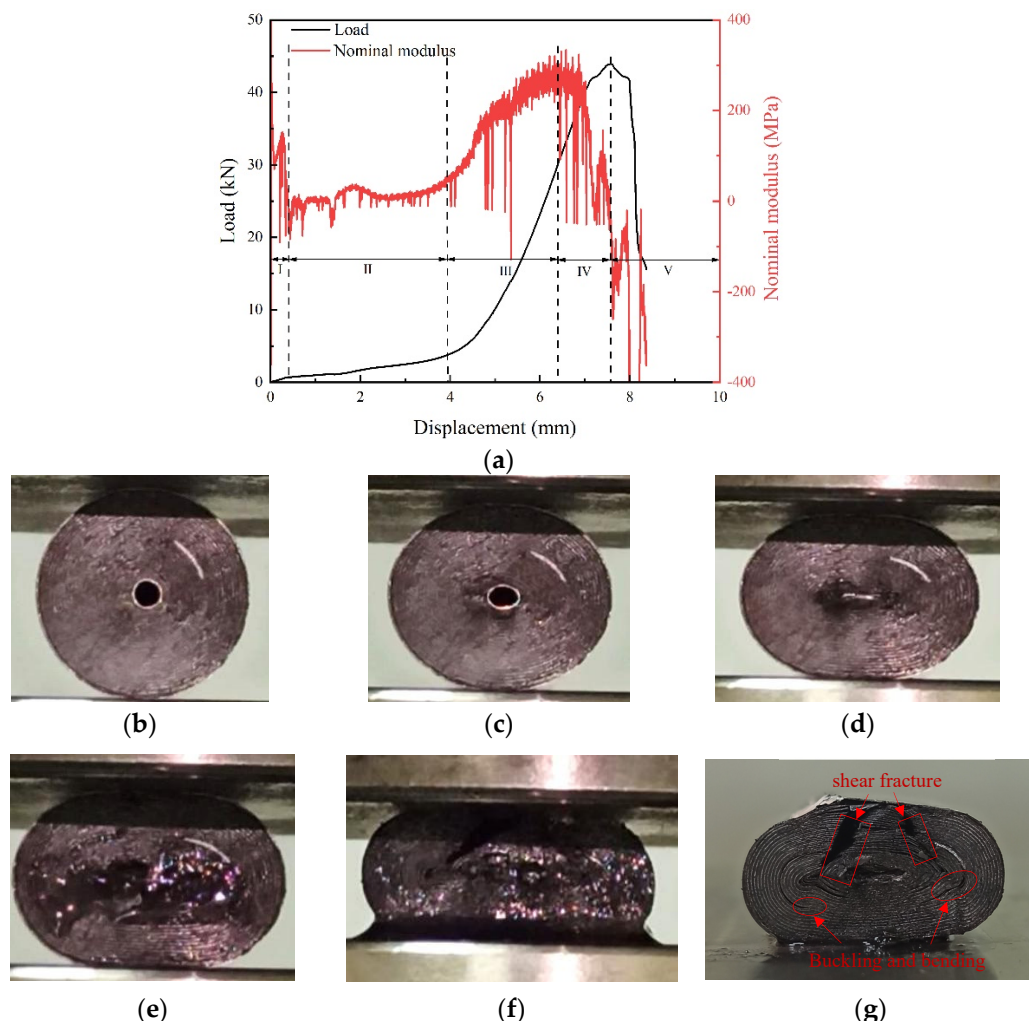


**Figure 5.** Radial compression process of power battery: (a) load, nominal modulus–displacement curve; (b) 0.4 mm deformation of Stage I; (c,d) 1.5 mm and 3.0 mm deformations diagram of Stage II; (e) 6.39 mm deformation diagram of Stage III; (f) 7.56 mm deformation diagram of Stage IV; (g) deformation diagram of Stage V.

The loading process was divided into five stages according to the nominal modulus. In Stage I, the battery just began to deform, and the steel casing resisted the load, as shown in Figure 5b. In Stage II, the load growth slowed due to the deformation of the hollow cylindrical steel core in the middle of the battery. The cylindrical steel core was the weakest part during this stage and was eventually compressed to closure, as shown in Figure 5c,d. In Stage III, with the core fully compacted, both the load and nominal modulus increased

with the displacement, and the internal electrolyte was gradually squeezed out, as shown in Figure 5e. When the compression displacement was about 6.39 mm, the nominal modulus reached the maximum value. In Stage IV, the load still increased with the displacement, but the nominal modulus started to decrease, and the electrolyte was poured out continuously, as shown in Figure 5f. In Stage V, the battery was severely damaged, and lost the load-bearing capacity. Cracks in the cross-section of the battery could be clearly seen in the recovered sample, as shown in Figure 5g. It can be seen that the final failure modes of the battery in radial plate compression were interlaminar fractures, local buckling, and bending deformation.

### 3.2. Influence of Radial Deformation on Capacity and Safety

In the radial compression test, voltage drop was taken as the criterion of battery failure. It was found that short circuit failure occurred only after the deformation of the battery reached 6 mm. Therefore, the influence of different deformations on battery life was considered. The battery was radially loaded and compressed to the specified deformation. The battery without a short circuit was charged and discharged in cycles according to the operation requirements in the manual. The health status of the battery was studied by analyzing the attenuation degree of the battery capacity in the cycling charge and discharge process.

Multiple groups of 40% SOC batteries were used for radial loading. The battery was loaded to the different deformation, and the loading rate was 2 mm/min. After unloading, the residual battery deformation was 0.42 mm, 1.08 mm, 2.74 mm, 2.80 mm, 3.20 mm, and 3.36 mm, as shown in Figure 6, and charge and discharge cycles were carried out on the battery without an internal short circuit. Observation of the deformed lithium-ion battery revealed that the positive and negative caps of the deformed battery were deformed and protruded outward.



**Figure 6.** Deformed batteries: (a) positive electrode; (b) negative electrode.

Figure 7 was a capacity–cycle curve plot obtained after fifty cycles of charge and discharge of six batteries with different deformation amounts. The charge–discharge cycle adopted the mode of CC–CV, and the charge rate was 0.2 C, and the specific charging method was stated in Section 2.2. The nominal capacity of the battery used in the experiment was 2.5 Ah. When comparing the initial points of each curve, it was found that the initial capacity value of the deformed batteries was reduced, and the larger the deformation, the smaller the initial capacity. Observing the trends in the curves, it was found that the larger the battery deformation, the faster the capacity reduction over the charge cycles. Based on the analysis of the battery structure and its working principle, we postulate that the following reasons might lead to large attenuation of battery capacity.

The electrodes of lithium ions are porous structures, and the analysis of Figure 4b in Section 3.1 shows that the mechanical properties of the battery are similar to those of porous materials. After radial compression, the electrode structure of the battery would have been deformed and damaged to some extent, leading to decreased embedding and mobility of lithium ions, thus reducing the specific capacity of the battery. Furthermore, when the battery was squeezed, the porosity of the separator would change, which would reduce the pass rate of lithium ions and affect the capacity of the battery.

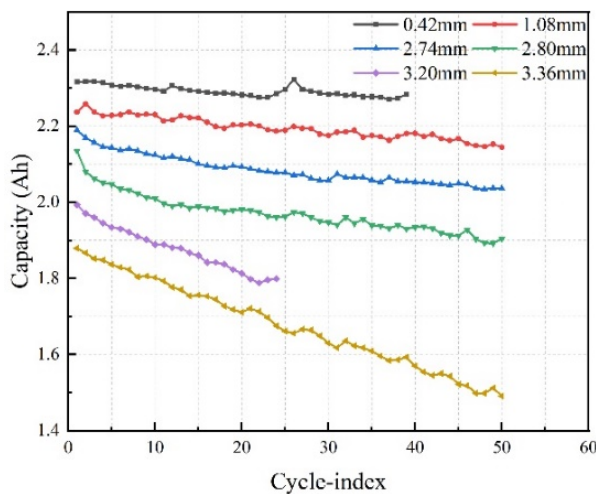


**Figure 7.** Capacity decay curves of batteries with 6 different residual deformations.

### 3.3. Influence of Axial Deformation on Capacity and Safety

The axial loading process is usually divided into four stages [5,6]: In the first stage, the groove between the positive cap and the jellyroll was squeezed, with the top and bottom edges of the groove folded to touch. In the second stage, the jellyroll joined the resistance to the load and was deformed to local buckling with indentations. In the third stage, the battery was further compressed, and the damage to the jellyroll increased. In the fourth stage, as the overall deformation of the battery further increased, short circuiting occurred and became more serious.

Figure 8 shows the load, voltage, and temperature–displacement curves of 40% SOC and 80% SOC batteries under 2 mm/min quasi-static loading. It can be concluded that the safety limit for the axial deformation is about 2.3 mm. At about 2.3 mm, the voltage of the 40% SOC battery had only a small drop and small temperature rise, but the voltage of the 80% SOC battery dropped to 0 V and thermal runaway occurred. This showed that batteries with higher SOC were more sensitive to deformation damage and would yield more Joule heat and thermal runaway in earlier stages.

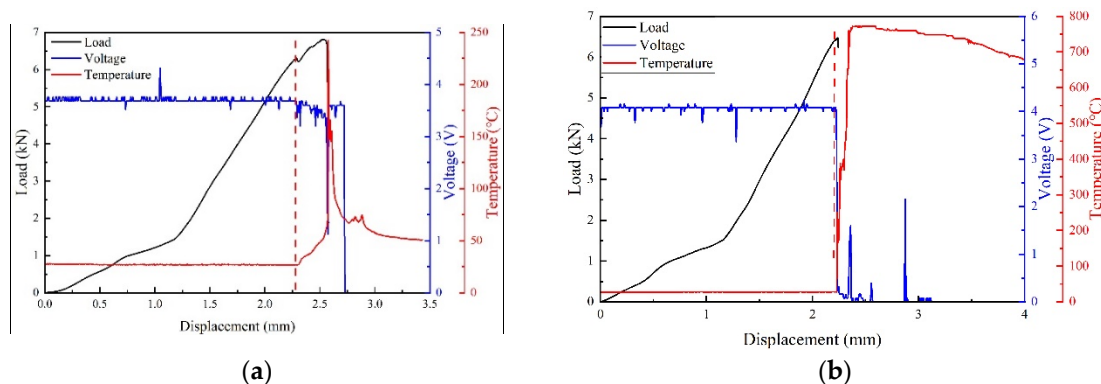


**Figure 8.** Load, voltage, and temperature–displacement curves of batteries with different SOCs: (a) 40%; (b) 80%.

In order to understand the influence of deformation on battery safety, the battery with 0% SOC was loaded at a rate of 2 mm/min to the sudden drop of voltage and stopped. The load, voltage, and temperature–displacement curves obtained are shown in Figure 9a. It was found that the battery voltage continued to decrease after the loading was stopped and quickly dropped to near zero, while the temperature continued to rise. Figure 9b shows the CT scan image of the battery after loading. The top of the jellyroll was squeezed and

bent. The failure of the battery was mainly caused by the contact between the anode and cathode materials due to the compression of the jellyroll, resulting in the voltage drop and total battery failure.

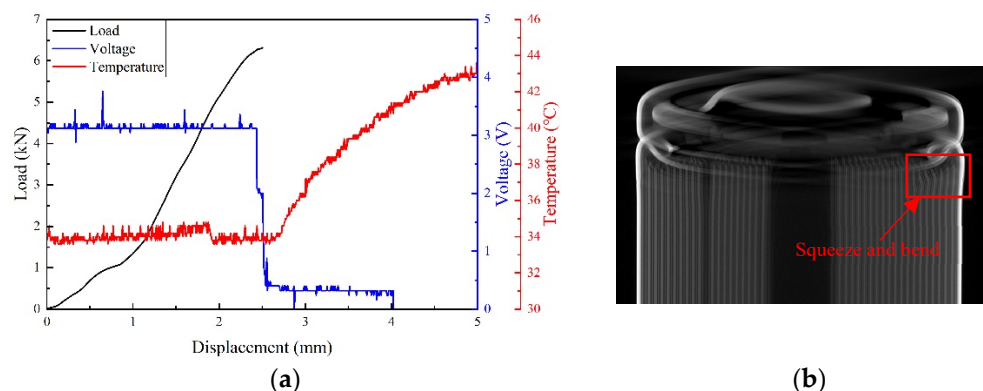


**Figure 9.** (a) Load, voltage, and temperature–displacement curve for the first voltage drop; (b) CT scan.

### 3.4. Comparison of the Two Types of Deformation on Battery Safety and Capacity

When comparing the response to the axial and radial deformation, it was found that the initial capacity of the battery decreased with the battery deformation under the radial plate compression, and the battery capacity decayed faster as the number of charging and discharging cycles increased. If the battery lateral residual deformation remained less than or equal to 3.36 mm, it could still be recharged, with little impact on its safety performance. However, in the axially loaded battery, the jellyroll came in contact with the positive and negative cap under less deformation, resulting in electrode folding and voltage drop; thus, Joule heat aggregation led to thermal runaway of the high-SOC battery.

Figure 10 shows the values of battery deformation when the complete voltage drop occurred under the two different loading modes. Compared with radial deformation, a smaller axial deformation caused battery failure and thermal runaway, resulting in lower battery safety. This was because of the different effects of the deformation modes on the battery electrode sheets and separators. When loaded laterally, the jellyroll is not easy to bend relatively, and the electrode sheets and separators will be constantly compacted during the compression process, with the load-bearing capacity increased. In contrast, under axial loading, the battery behaves as a thin-walled cylindrical shell under compression, deforming with buckling wrinkles with excessive local bending, which easily causes damage.

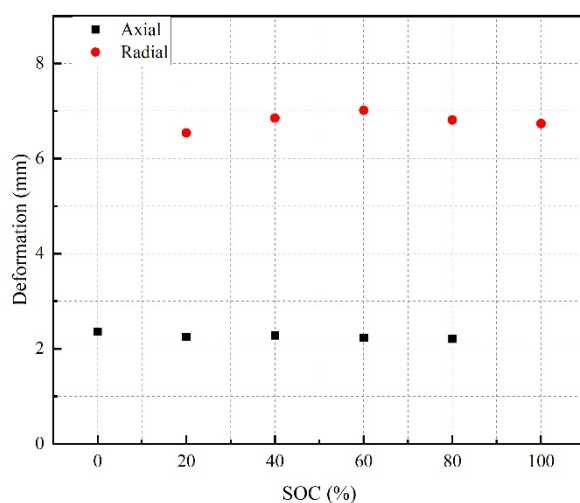


**Figure 10.** Failure displacement of power battery under different loads.

#### 4. Conclusions

In this study, the axial and radial loading of lithium-ion batteries with different SOC were performed. The failure modes of the batteries under the two loading modes and the influence of deformation on their safety performance and capacity were discussed. The results are presented below.

1. It was found that the deformation process of the battery under radial compression could be divided into five stages. Stage I and Stage II were for the steel shell and steel core to resist the load, respectively. In Stage III and Stage IV, the jellyroll resisted the load, the electrolyte was squeezed out, and the nominal modulus of the cell reached its maximum at the end of Stage III. In Stage V, the battery was severely damaged and cracks appeared; interlayer fracture and local buckling were found in the failure modes of the battery.
2. When loaded axially, the voltage of the battery fell step by step. When the jellyroll was subjected to local indentation, the electrode was squeezed and bent, the voltage dropped slightly, and continued to drop to zero after loading was stopped, and the battery failed.
3. The radial deformation reduced the capacity of the battery; the initial capacity decreased more as the deformation increased, and the capacity decayed constantly with as the number of charge–discharge cycles increased. However, the local deformation of the jellyroll caused by axial loading resulted in battery failure, but did not affect the electrode material structure and had little impact on the capacity.
4. When the radial residual deformation was less than or equal to 3.36 mm, the battery could undergo normal charging and discharging cycle without safety problems. However, when the axial deformation reached 2.3 mm, the battery failed, and even caused thermal runaway for a high-SOC lithium-ion battery, meaning that the battery was more sensitive to axial deformation.

The results of the study reveal the influence of deformation on the battery, which has notable significance for judging the safety performance of the battery and the safe arrangement of battery packs.

**Author Contributions:** Conceptualization, G.W. and B.W.; methodology, G.W.; software, J.W.; validation, G.W. and J.W.; formal analysis, J.W.; investigation, G.W., J.W., Z.Z., L.N. and L.P.; resources, G.W.; data curation, J.W., Z.Z., L.N. and L.P.; writing—original draft preparation, G.W. and J.W.; writing—review and editing, G.W. and B.W.; visualization, J.W.; supervision, G.W. and B.W.; project administration, G.W.; funding acquisition, G.W. All authors have read and agreed to the published version of the manuscript.

**Funding:** This research was funded by the National Natural Science Foundation of China (Grant Number 11872265), the Central Guidance on Local Science and Technology Development Fund of Shanxi Province (YDZJSX2021A021), and the Natural Science Foundation of Shanxi Province (Grant Number 201901D111087).

**Data Availability Statement:** Not applicable.

**Conflicts of Interest:** The authors declare no conflict of interest.

#### References

1. Ruiz, V.; Pfrang, A.; Kriston, A.; Omar, N.; Van den Bossche, P.; Boon-Brett, L. A Review of International Abuse Testing Standards and Regulations for Lithium Ion Batteries in Electric and Hybrid Electric Vehicles. *Renew. Sustain. Energy Rev.* **2018**, *81*, 1427–1452. [[CrossRef](#)]
2. IEC 62133.2-2017; Secondary Cells and Batteries Containing Alkaline or Other Non-Acid Electrolytes-Secondary Lithium Cells and Batteries for Portable Applications-Part 3: Prismatic and Cylindrical Lithium Secondary Cells and Batteries Made. International Electrotechnical Commission, Swiss Confederation: Geneva, Switzerland, 2017.
3. Xi, S.; Zhao, Q.; Chang, L.; Huang, X.; Cai, Z. The Dynamic Failure Mechanism of a Lithium-Ion Battery at Different Impact Velocity. *Eng. Fail. Anal.* **2020**, *116*, 104747. [[CrossRef](#)]
4. Fan, W.; Xue, P.; Wang, G.; Wang, B. Safety performance of lithium-ion battery under compressive load(in Chinese). *Chin. J. High Press. Phys.* **2019**, *33*, 065901(1)–065901(7). [[CrossRef](#)]

5. Zhu, J.; Zhang, X.; Sahraei, E.; Wierzbicki, T. Deformation and Failure Mechanisms of 18650 Battery Cells under Axial Compression. *J. Power Sources* **2016**, *336*, 332–340. [[CrossRef](#)]
6. Wang, G.; Zhang, S.; Li, M.; Wu, J.; Wang, B.; Song, H. Deformation and Failure Properties of High-Ni Lithium-Ion Battery under Axial Loads. *Materials* **2021**, *14*, 7844. [[CrossRef](#)] [[PubMed](#)]
7. Yang, S.; Wang, W.; Lin, C.; Shen, W.; Li, Y. Investigation of Internal Short Circuits of Lithium-Ion Batteries under Mechanical Abusive Conditions. *Energies* **2019**, *12*, 1885. [[CrossRef](#)]
8. Wang, W.; Yang, S.; Lin, C.; Shen, W.; Lu, G.; Li, Y.; Zhang, J. Investigation of Mechanical Property of Cylindrical Lithium-Ion Batteries under Dynamic Loadings. *J. Power Sources* **2020**, *451*, 227749. [[CrossRef](#)]
9. Wang, L. Deformation and Failure Properties of Lithium-Ion Battery Under Axial Nail Penetration. *J. Electrochem. Energy Convers. Storage* **2021**, *18*, 020906. [[CrossRef](#)]
10. Wang, L.; Yin, S.; Xu, J. A Detailed Computational Model for Cylindrical Lithium-Ion Batteries under Mechanical Loading: From Cell Deformation to Short-Circuit Onset. *J. Power Sources* **2019**, *413*, 284–292. [[CrossRef](#)]
11. Greve, L.; Fehrenbach, C. Mechanical Testing and Macro-Mechanical Finite Element Simulation of the Deformation, Fracture, and Short Circuit Initiation of Cylindrical Lithium Ion Battery Cells. *J. Power Sources* **2012**, *214*, 377–385. [[CrossRef](#)]
12. Zhang, H.; Zhou, M.; Hu, L.; Zhang, Z. Mechanism of the Dynamic Behaviors and Failure Analysis of Lithium-Ion Batteries under Crushing Based on Stress Wave Theory. *Eng. Fail. Anal.* **2020**, *108*, 104290. [[CrossRef](#)]
13. Avdeev, I.; Gilaki, M. Structural Analysis and Experimental Characterization of Cylindrical Lithium-Ion Battery Cells Subject to Lateral Impact. *J. Power Sources* **2014**, *271*, 382–391. [[CrossRef](#)]
14. Xu, J.; Liu, B.; Wang, X.; Hu, D. Computational Model of 18650 Lithium-Ion Battery with Coupled Strain Rate and SOC Dependencies. *Appl. Energy* **2016**, *172*, 180–189. [[CrossRef](#)]
15. Xu, J.; Jia, Y.; Liu, B.; Zhao, H.; Yu, H.; Li, J.; Yin, S. Coupling Effect of State-of-Health and State-of-Charge on the Mechanical Integrity of Lithium-Ion Batteries. *Exp. Mech.* **2018**, *58*, 633–643. [[CrossRef](#)]
16. Xu, J.; Liu, B.; Hu, D. State of Charge Dependent Mechanical Integrity Behavior of 18650 Lithium-Ion Batteries. *Sci. Rep.* **2016**, *6*, 21829. [[CrossRef](#)] [[PubMed](#)]
17. Wang, W.; Li, Y.; Lin, C.; Yang, S. State of Charge-Dependent Failure Prediction Model for Cylindrical Lithium-Ion Batteries under Mechanical Abuse. *Appl. Energy* **2019**, *251*, 113365. [[CrossRef](#)]
18. Li, B.; Jones, C.M.; Adams, T.E.; Tomar, V. Sensor Based In-Operando Lithium-Ion Battery Monitoring in Dynamic Service Environment. *J. Power Sources* **2021**, *486*, 229349. [[CrossRef](#)]
19. Spielbauer, M.; Berg, P.; Ringat, M.; Bohlen, O.; Jossen, A. Experimental Study of the Impedance Behavior of 18650 Lithium-Ion Battery Cells under Deforming Mechanical Abuse. *J. Energy Storage* **2019**, *26*, 101039. [[CrossRef](#)]
20. Müller, V.; Scurtu, R.-G.; Memm, M.; Danzer, M.A.; Wohlfahrt-Mehrens, M. Study of the Influence of Mechanical Pressure on the Performance and Aging of Lithium-Ion Battery Cells. *J. Power Sources* **2019**, *440*, 227148. [[CrossRef](#)]
21. Zhu, X.; Wang, H.; Wang, X.; Gao, Y.; Allu, S.; Cakmak, E.; Wang, Z. Internal Short Circuit and Failure Mechanisms of Lithium-Ion Pouch Cells under Mechanical Indentation Abuse Conditions: An Experimental Study. *J. Power Sources* **2020**, *455*, 227939. [[CrossRef](#)]
22. Zhu, X.; Wang, H.; Allu, S.; Gao, Y.; Cakmak, E.; Hopkins, E.J.; Veith, G.M.; Wang, Z. Investigation on Capacity Loss Mechanisms of Lithium-Ion Pouch Cells under Mechanical Indentation Conditions. *J. Power Sources* **2020**, *465*, 228314. [[CrossRef](#)]
23. Shao, Y.; Jin, Z.; Li, J.; Meng, Y.; Huang, X. Evaluation of the Electrochemical and Expansion Performances of the Sn-Si/Graphite Composite Electrode for the Industrial Use. *Energy Mater.* **2022**, *2*, 200004. [[CrossRef](#)]
24. Heng, Y.-L.; Gu, Z.-Y.; Guo, J.-Z.; Yang, X.-T.; Zhao, X.-X.; Wu, X.-L. Research Progress on the Surface/Interface Modification of High-Voltage Lithium Oxide Cathode Materials. *Energy Mater.* **2022**, *2*, 200017. [[CrossRef](#)]
25. Yue, L.; Ma, C.; Yan, S.; Wu, Z.; Zhao, W.; Liu, Q.; Luo, Y.; Zhong, B.; Zhang, F.; Liu, Y.; et al. Improving the Intrinsic Electronic Conductivity of NiMoO<sub>4</sub> Anodes by Phosphorous Doping for High Lithium Storage. *Nano Res.* **2022**, *15*, 186–194. [[CrossRef](#)]
26. Yue, L.; Liang, J.; Wu, Z.; Zhong, B.; Luo, Y.; Liu, Q.; Li, T.; Kong, Q.; Liu, Y.; Asiri, A.M.; et al. Progress and Perspective of Metal Phosphide/Carbon Heterostructure Anodes for Rechargeable Ion Batteries. *J. Mater. Chem. A* **2021**, *9*, 11879–11907. [[CrossRef](#)]
27. Li, C.; Liu, B.; Jiang, N.; Ding, Y. Elucidating the Charge-Transfer and Li-Ion-Migration Mechanisms in Commercial Lithium-Ion Batteries with Advanced Electron Microscopy. *Nano Res. Energy* **2022**, *1*, e9120031. [[CrossRef](#)]
28. Mallarapu, A.; Kim, J.; Carney, K.; DuBois, P.; Santhanagopalan, S. Modeling Extreme Deformations in Lithium Ion Batteries. *eTransportation* **2020**, *4*, 100065. [[CrossRef](#)]
29. Liu, H.; Naqvi, I.H.; Li, F.; Liu, C.; Shafiei, N.; Li, Y.; Pecht, M. An Analytical Model for the CC-CV Charge of Li-Ion Batteries with Application to Degradation Analysis. *J. Energy Storage* **2020**, *29*, 101342. [[CrossRef](#)]